

**Smectic ordering in liquid-crystal–aerosil dispersions. I. X-ray scattering**R. L. Leheny,<sup>1</sup> S. Park,<sup>2,\*</sup> R. J. Birgeneau,<sup>2,3</sup> J.-L. Gallani,<sup>2,†</sup> C. W. Garland,<sup>2</sup> and G. S. Iannacchione<sup>4</sup><sup>1</sup>*Department of Physics and Astronomy, Johns Hopkins University, Baltimore, Maryland 21218*<sup>2</sup>*Center for Materials Science and Engineering, Massachusetts Institute of Technology, Cambridge, Massachusetts 02139*<sup>3</sup>*Department of Physics, University of Toronto, Toronto, Ontario, Canada M5S 1A1*<sup>4</sup>*Department of Physics, Worcester Polytechnic Institute, Worcester, Massachusetts 01609*

(Received 8 July 2002; published 31 January 2003)

Comprehensive x-ray scattering studies have characterized the smectic ordering of octylcyanobiphenyl (8CB) confined in the hydrogen-bonded silica gels formed by aerosil dispersions. For all densities of aerosil and all measurement temperatures, the correlations remain short range, demonstrating that the disorder imposed by the gels destroys the nematic (*N*) to smectic-*A* (Sm*A*) transition. The smectic correlation function contains two distinct contributions. The first has a form identical to that describing the critical thermal fluctuations in pure 8CB near the *N*-Sm*A* transition, and this term displays a temperature dependence at high temperatures similar to that of the pure liquid crystal. The second term, which is negligible at high temperatures but dominates at low temperatures, has a shape given by the thermal term squared and describes the static fluctuations due to random fields induced by confinement in the gel. The correlation lengths appearing in the thermal and disorder terms are the same and show a strong variation with gel density at low temperatures. The temperature dependence of the amplitude of the static fluctuations further suggests that nematic susceptibility becomes suppressed with increasing quenched disorder. The results overall are well described by a mapping of the liquid-crystal–aerosil system onto a three-dimensional *XY* model in a random field with disorder strength varying linearly with the aerosil density.

DOI: 10.1103/PhysRevE.67.011708

PACS number(s): 61.30.Pq, 61.30.Eb, 64.70.Md, 61.10.Eq

**I. INTRODUCTION**

Liquid crystals have long served as important model systems in statistical mechanics. For example, experiments on phase transitions in liquid crystals have provided many of the most detailed tests of the modern theories of critical phenomena. Recent studies in liquid crystals have investigated the effects that quenched disorder produces in phase behavior and mesophase ordering, and a fruitful strategy in experiments for introducing quenched disorder has been through confinement in random porous media. The fragile nature of the mesomorphic phases and the importance of surface interactions make such a confinement particularly well suited for liquid-crystalline systems. For example, a series of experiments [1–5] has characterized the effects on the nematic to isotropic and nematic to smectic-*A* transitions of liquid crystals confined in aerogels—highly porous, chemically bonded silica gels. The primary conclusion of this work has been that the transition behavior becomes severely smeared and that long-range nematic and smectic ordering is suppressed by the aerogel. In particular, these studies have verified theoretical expectations about the fragility of the smectic phase to disorder [6].

In order to access a weaker regime of disorder than is possible with aerogel or other rigid porous media, several recent studies have focused on liquid crystals confined within aerosil gels—weak, thixotropic gels comprised of nanometer scale silica particles. The disorder imposed by aerosil gels can be made less severe than in the case of aerogels,

both because lower volume fractions are possible with aerosils and because the compliance of the aerosil gels leads to partial annealing of the disorder. This work on liquid crystals in aerosil dispersions, including calorimetry [7], nuclear magnetic resonance [8], dielectric susceptibility [9], and static light scattering [10], has revealed important differences between such systems and liquid crystals in aerogels, which can be ascribed to the weaker nature of the aerosil disorder. In particular, an x-ray scattering investigation into the nematic to smectic-*A* transition in a prototypical thermotropic liquid crystal, octylcyanobiphenyl (8CB), in the presence of dispersed aerosil gels has shown that the aerosil gel can be quantitatively understood as introducing weak-to-intermediate strength random fields that compete with smectic ordering in the liquid crystal [11].

Random-field systems have been fruitful models for exploring effects of quenched disorder, and experimentally, random-field Ising magnets have been at the center of this work [12]. The nematic to smectic transition breaks a three-dimensional (3D) *XY* symmetry; thus 8CB with dispersed aerosils provides an opportunity to study experimentally a random-field system that breaks a continuous symmetry [13–18]. In this paper we provide a comprehensive picture of the smectic correlations in 8CB confined in aerosil gels, as determined by the x-ray scattering. The analysis we apply adopts a random-field picture, and consistent with theoretical predictions for a 3D *XY* system with random fields, we find that the smectic phase is destroyed by the disorder and is replaced by the growth of short-range smectic correlations. The results in this paper build on the preliminary findings of Ref. [11], providing a refined and greatly extended analysis of the x-ray data including detailed comparisons with theory. A feature of these x-ray results and corresponding calorimet-

\*Present address: NCNR, NIST, Gaithersburg, MD.

†Permanent address: IPCMS-GMO, Strasbourg, France.

ric studies [7] worth noting is the lack of any measurable hysteresis or time-dependent effects that would indicate out-of-equilibrium behavior. In the random-field Ising magnet, slow dynamics and metastability [19,20] severely complicate efforts to understand the underlying equilibrium behavior. The observed absence of such problems for the nematic to smectic transition in aerosil, presumably a consequence of the system's continuous symmetry, indicates an opportunity to view equilibrium behavior in a random-field system. The companion paper that follows this paper [21], hereafter called Paper II, compares the x-ray and calorimetry results to reveal scaling behavior in the smectic ordering in the presence of the aerosil gel.

Recent theoretical work has emphasized the strong effect of confinement in random media on liquid-crystal phases [17,18,22–24]. A detailed study by Radzihovsky and Toner [17], which models the confinement as introducing random fields, has predicted the destruction of the smectic-*A* phase by arbitrarily weak quenched disorder, consistent with experiment, and has introduced the possibility that a topologically ordered “smectic Bragg glass” phase may appear at low temperatures. The smectic Bragg glass is a possible manifestation of the anomalous elasticity that the theory predicts for the smectic phase in the presence of disorder. Distinguishing features of this anomalous elasticity and smectic Bragg glass phase are the smectic correlations in the system. Thus, x-ray scattering, which can directly probe the smectic correlation function, is an ideal probe for testing some of these ideas, and recent analysis of x-ray studies on 8CB in aerogels has been reported to show agreement with many of these predictions [6]. The weaker nature of disorder from aerosil gels should place 8CB+aerosil samples more firmly in the regime addressed by the theory. However, as shown in the present work, the agreement between the observed smectic correlations in 8CB in aerosil gels and more detailed predictions of the theory is limited.

Section II of this paper describes the sample preparation and the details of the x-ray scattering measurements on 8CB in aerosil gels, and Sec. III outlines the results of the x-ray line-shape analysis, which yields insight into both thermal and static smectic fluctuations and the temperature dependence of correlation lengths and smectic susceptibilities. Section IV provides a discussion of the pseudocritical structural behavior of 8CB in weak aerosil gels. Paper II extends this discussion with the analysis of scaling behavior and comparisons with calorimetry.

## II. EXPERIMENTAL PROCEDURES

### A. Sample preparation and characteristics

The 8CB used in this study came from a single synthetic batch obtained from Aldrich Corp. The liquid crystal had a quoted purity of 99% and was used without further purification. In the absence of disorder, pure 8CB undergoes an isotropic (*I*) to nematic (*N*) transition at  $T_{NI}^0 = 313.98$  K and a nematic to smectic-*A* (*SmA*) transition at  $T_{NA}^0 = 306.97$  K [7]. Below 290 K, 8CB forms a three-dimensional ordered crystal phase. The aerosil, obtained from Degussa Corp.,

consists of 70-Å-diameter SiO<sub>2</sub> spheres, and the type 300 aerosil used in this study is strongly hydrophilic.

The aerosil gels were formed directly in the liquid crystal following established procedures [7]. Appropriate quantities of degassed 8CB and dried aerosil powder were mixed with high purity acetone, and the suspensions were sonicated for several hours to achieve a uniform dispersion. The suspensions were then gently heated to 315 K to evaporate the acetone slowly. After no signs of acetone remained, the samples were placed under vacuum at  $10^{-2}$  Torr for 12 h at 320 K to remove any trace amounts of solvent or absorbed water vapor. For aerosil densities above a gelation threshold of  $\approx 1\%$  silica by volume, the resulting material was a highly uniform soft solid that maintained its shape when heated above  $T_{NI}^0$ . Small-angle x-ray scattering has revealed that aerosil gels formed under this procedure bear a strong resemblance to rigid aerogels [1,7]. Paper II provides a detailed discussion of the gel structure formed by aerosils, including an account of its characteristic length scales and their dependence on density as well as a description of the similarities and differences with the more extensively studied aerogel system. The samples in this study ranged in aerosil densities from  $\rho_S = 0.025$  g silica/cm<sup>3</sup> 8CB, which is just above the gelation threshold, to  $\rho_S = 0.341$  g silica/cm<sup>3</sup> 8CB. Several efforts to prepare samples below the threshold density produced macroscopically inhomogeneous materials that were unsuitable for study.

### B. X-ray scattering

The x-ray scattering studies were conducted on the X20A and X20C beam lines of the National Synchrotron Light Source at Brookhaven National Laboratory using 8-keV x rays. The samples were placed in aluminum holders with epoxy-sealed Kapton windows designed to maintain a sample thickness of  $\approx 1$  mm, closely matching the attenuation length for the 8-keV radiation through the material. The holders were mounted in a brass block, which in turn was positioned in a beryllium can containing dry nitrogen gas. A thermoelectric cooler mounted on top of the beryllium can in conjunction with a resistive heater powered by a home-built P-I temperature controller maintained a set temperature for the brass block. Preliminary x-ray scattering measurements showed that the crystallization of 8CB was suppressed  $\approx 7$  K by confinement in aerosil gels. Because such crystallization irreversibly damages the aerosil gels, we limited our studies to temperatures safely above this point. The measurement temperatures ranged from 287 K,  $\approx 20$  K below the *N*-*SmA* transition in pure 8CB, to 318 K,  $\approx 4$  K above the *N*-*I* transition. The temperature stability during a measurement was better than  $\pm 0.001$  K.

The scattering intensity was measured in transmission in a vertical scattering geometry. The scattered beam was reflected from a single-crystal germanium analyzer to achieve high wave-vector resolution and was measured with a point scintillation detector. Because the scattering intensity from the liquid-crystal-aerosil gel composites had the azimuthal symmetry of a powder pattern, two sets of slits between the sample and the analyzer were used to define tightly the hori-

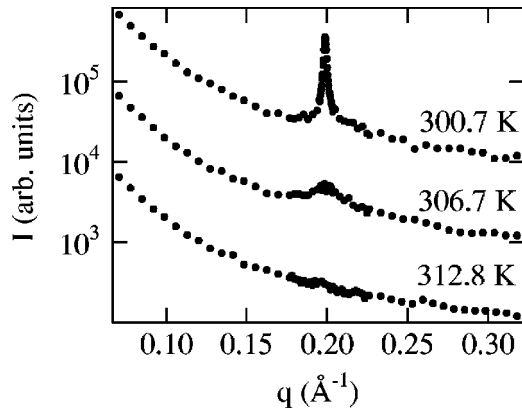


FIG. 1. Scattering intensity for 8CB in an aerosil gel with  $\rho_S = 0.161 \text{ g/cm}^3$  at three temperatures spanning the  $N$ -SmA transition of the pure system,  $T_{NA}^0 = 306.97 \text{ K}$ . The curves for 300.7 K and 306.7 K have been shifted by factors of 100 and 10, respectively, for clarity. The strongly temperature-dependent peak near  $q = 0.2 \text{ \AA}^{-1}$  corresponds to scattering from smectic modulations.

zonal acceptance, and thus provide an undistorted measurement of the scattering intensity as a function of wave-vector transfer,  $I(q)$  [25].

Preliminary measurements of the scattering from 8CB+aerosil samples revealed damage to the material from prolonged exposure to the x-ray radiation. This damage was reflected in irreproducibility in the observed  $I(q)$  and a progressive temperature shift in the onset of the short-ranged smectic order described in Sec. III D. To combat this problem a protocol was developed, which made these effects immeasurably small. Immediately after the sample was loaded into the scattering cell and before any x-ray measurements were made, the material was heated to  $\approx 318 \text{ K}$ , several degrees above  $T_{NI}^0$ . The material was then cooled through a series of temperatures at which measurements of the scattering intensity  $I(q)$  were made. A process of trial-and-error during preliminary studies revealed the appropriate exposure times for the final measurements to optimize statistics while avoiding measurable damage. After the series of measurements ending at the lowest temperature was complete, the material was reheated and measurements were repeated at several temperatures to assure that no measurable changes in the scattering had occurred. Finally, the material was heated back to 318 K, and a measurement with a long counting time was conducted to determine the background scattering from the aerosil gel structure.

### III. RESULTS

#### A. Line-shape analysis

Figure 1 displays representative results for  $I(q)$  from a sample with  $\rho_S = 0.161 \text{ g/cm}^3$  at three temperatures spanning the  $N$ -SmA transition temperature in pure 8CB,  $T_{NA}^0 = 306.97 \text{ K}$ . The scattering line shape contains two salient features: a broad, sloping background that is approximately temperature independent and a strongly temperature-dependent peak that develops on cooling near  $0.2 \text{ \AA}^{-1}$ . The background consists primarily of scattering from the aerosil

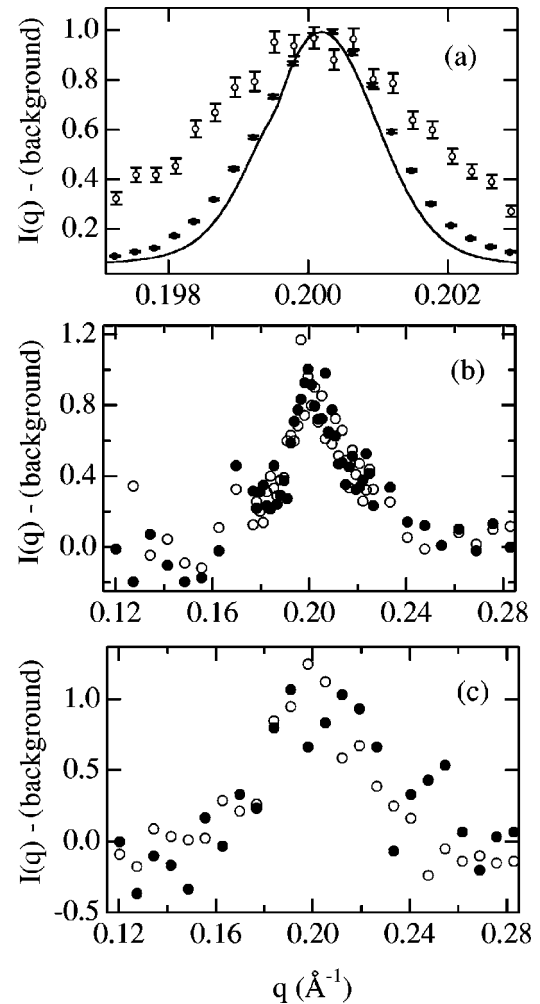


FIG. 2. Comparison of the smectic Bragg peak measured for 8CB in aerosil gels with that measured for pure 8CB. All peak heights have been normalized to 1. (a) At low temperature ( $T_{NA}^0 - 19 \text{ K}$  shown here) the width of the peak for pure 8CB (line) is essentially identical to that set by the experimental resolution, as determined from the direct x-ray beam profile. The wider peaks measured for 8CB in aerosil gels with  $\rho_S = 0.025 \text{ g/cm}^3$  (solid circles) and  $\rho_S = 0.220 \text{ g/cm}^3$  (open circles) indicate that the smectic correlations remain short-ranged to low temperatures due to the disorder imposed by the gels. (b),(c) Above  $T_{NA}^0$ , the line shapes measured for 8CB in aerosil gels and those measured for pure 8CB are indistinguishable: (b)  $\rho_S = 0.078 \text{ g/cm}^3$  (solid circles) and pure 8CB (open circles) each at 308.3 K; and (c)  $\rho_S = 0.031 \text{ g/cm}^3$  (solid circles) at 310.8 K and pure 8CB (open circles) at 310.5 K.

gel structure. The temperature-dependent peak results from smectic modulations in the 8CB. The shape of this peak is a direct measure of the smectic correlation function for the 8CB confined in the aerosil gel.

For the full range of aerosil densities and to the lowest measurement temperatures, the observed smectic peak is significantly broader than the resolution limit set by the x-ray optics, as illustrated in Fig. 2(a). Measurements of pure 8CB below  $T_{NA}^0$ , shown by the solid line in the figure, revealed a line shape whose width is virtually indistinguishable from that of the resolution, which we determined from the shape of the profile of the direct x-ray beam. (The subtle increase in

width in pure 8CB due to the Landau-Peierls instability is not resolved.) The solid circles in Fig. 2(a) are the line shape measured for an 8CB+aerosil sample with  $\rho_S=0.025$ , the lowest aerosil density, at 287.8 K ( $T_{NA}^0 - 19.2$  K). The larger width of the aerosil peak with respect to the resolution reflects the finite extent of the smectic correlations in the presence of the aerosil gel, and the consequent destruction of the transition to a quasi-long-range ordered smectic state by the quenched disorder. The length scale for this short-range order depends strongly on  $\rho_S$ , as revealed by the contrast between the low-temperature width for the  $\rho_S=0.025$  sample and that for a  $\rho_S=0.220$  sample, shown by the open circles in Fig. 2(a).

To characterize these short-range correlations, we model the structure factor for the smectic ordering with the form

$$S(\mathbf{q}) = \frac{\sigma_1}{1 + (q_{\parallel} - q_0)^2 \xi_{\parallel}^2 + q_{\perp}^2 \xi_{\perp}^2 + c q_{\perp}^4 \xi_{\perp}^4} + \frac{a_2 (\xi_{\parallel} \xi_{\perp}^2)}{[1 + (q_{\parallel} - q_0)^2 \xi_{\parallel}^2 + q_{\perp}^2 \xi_{\perp}^2 + c q_{\perp}^4 \xi_{\perp}^4]^2}, \quad (1)$$

where the wave vector  $q_{\parallel}$  is along the smectic layer normal and  $q_{\perp}$  is perpendicular to it. The first term in  $S(q)$ , an anisotropic Lorentzian with quartic corrections, has the same form as the structure factor in pure nematic 8CB and represents the smectic susceptibility, with  $\sigma_1$  equal to the magnitude of the susceptibility at the ordering wave vector  $q_0$ . This term characterizes the critical thermal fluctuations on approaching the  $N$ -SmA transition [26]. The second term, whose shape is given by the susceptibility squared, is designed to account for the static fluctuations induced by the quenched disorder. This second term is motivated by studies on random-field systems. Such an expression, known as the disconnected susceptibility, has been shown to describe accurately the short-range correlations induced by the static fluctuations in random-field Ising magnets [27] and has been justified theoretically [28–30] for these systems. A very similar expression has also been derived specifically for smectic liquid crystals in the presence of random fields [18]. In the limit of long-range order, the second term evolves into a Bragg peak,  $a_2 \delta(q_{\parallel} - q_0) \delta(q_{\perp})$  [31]. In applying Eq. (1) to the smectic correlations of 8CB in aerosil gels,  $\xi_{\perp}$  and  $c$  are treated as functions of  $\xi_{\parallel}$ , with  $\xi_{\perp}(\xi_{\parallel})$  and  $c(\xi_{\parallel})$  set by their relations in pure 8CB, which are known to high precision [26].

The total measured scattering intensity is fit to the powder average of  $S(\mathbf{q})$  from Eq. (1), convolved with the resolution, plus a term to account for the background scattering from the aerosil gel shown in Fig. 1:

$$I(q) = \int dq' \int d\Omega S(\mathbf{q}') \text{Res}(q - q') + A(T)B(q). \quad (2)$$

The powder average, represented by the integral over solid angles, can be solved analytically for the  $S(\mathbf{q})$  form given by Eq. (1). The details of this calculation are provided in the

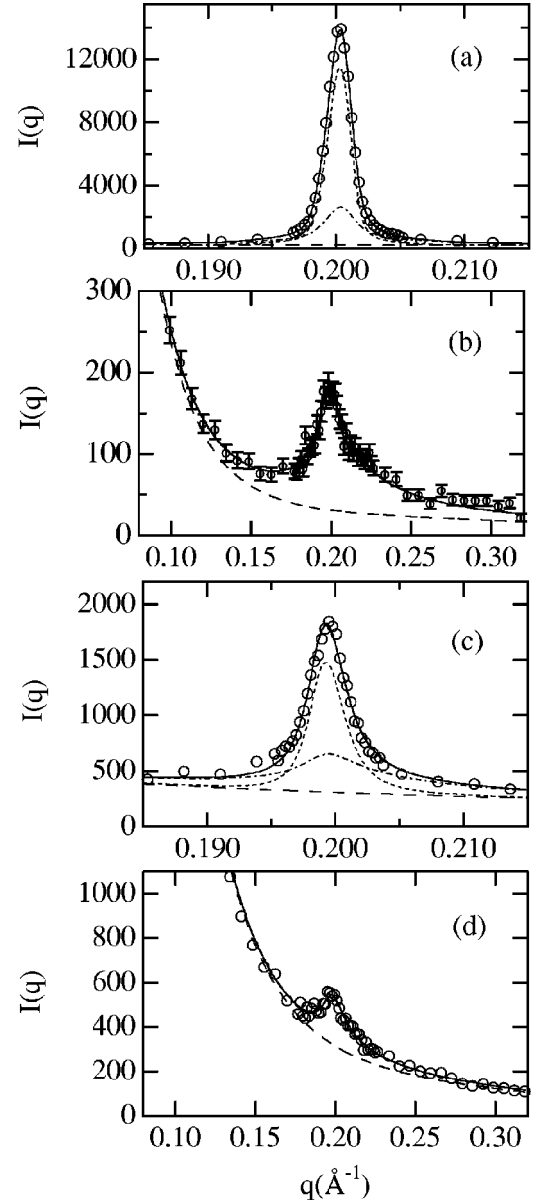


FIG. 3. Scattering intensity  $I(q)$  for 8CB in confined aerosil gels. (a)  $\rho_S=0.025$  g/cm<sup>3</sup> at 288.5 K, (b)  $\rho_S=0.025$  g/cm<sup>3</sup> at 307.6 K, (c)  $\rho_S=0.282$  g/cm<sup>3</sup> at 300.6 K, and (d)  $\rho_S=0.282$  g/cm<sup>3</sup> at 306.6 K. The solid line in each panel is a fit with Eqs. (1) and (2), and the dashed line is the background contribution from the aerosil gel structure. In panels (a) and (c), the dash-dotted line is the contribution from the first term in Eq. (1), representing thermal fluctuations, plus the background, and the dotted line is the second term, representing static fluctuations, plus the background. In panels (b) and (d), the temperatures are above a pseudotransition temperature  $T^*$  defined in Sec. III D, and the smectic correlations are described entirely by thermal fluctuations.

Appendix. The convolution with the resolution function,  $\text{Res}(q)$ , was performed numerically. The shape of the background,  $B(q)$ , was taken from measurements at a high temperature, where scattering from the aerosil gel dominates, and this quantity is multiplied by a temperature-dependent parameter  $A(T)$ , which accounts for variations in the scattering contrast between the silica and 8CB due to differences

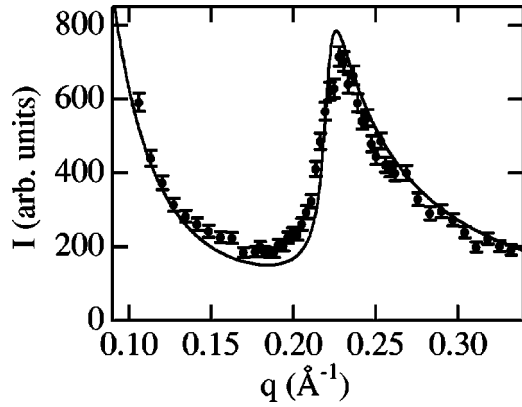


FIG. 4. Smectic peak measured for  $\bar{8}S5$  confined in an aerosil gel with  $\rho_S=0.030$  g/cm<sup>3</sup> at 339.04 K, 2.56 K above the  $N$ -SmA transition temperature of pure  $\bar{8}S5$ . The solid line is a fit with Eqs. (1) and (2), using values of  $\xi_{\perp}(\xi_{\parallel})$  and  $c(\xi_{\parallel})$  from pure  $\bar{8}S5$  and with  $a_2=0$ , so that only the thermal fluctuations are included in describing the smectic correlations. The strongly asymmetric line shape is a consequence of the powder averaging.

in their thermal expansion. We found that  $A(T)$  typically differed from unity by less than 10% over the full temperature range of the measurements.

At temperatures near and above  $T_{NA}^0$ , the measured line shapes in the aerosil samples are described very well by the thermal fluctuation term alone (i.e., fitted  $a_2$  are very small, and one can set  $a_2=0$  with almost no effect on the other parameters). Thus, for  $T>T_{NA}^0$ , the smectic correlations in aerosil samples are very similar to the critical fluctuations of the pure liquid crystal. This strong similarity is demonstrated in Figs. 2(b) and 2(c), which compare the smectic peak for two values of  $\rho_S$  with that measured for pure 8CB at temperatures several degrees above  $T_{NA}^0$ .

Figure 3 shows representative results for fits to the line shapes of two samples with Eqs. (1) and (2). The solid lines in the figure correspond to the full fit while the dotted, dash-dotted and dashed lines correspond to contributions made by each of the three terms, static fluctuations, thermal fluctuations, and background, respectively. As mentioned above, in the fits with Eq. (1),  $\xi_{\perp}$  and  $c$  are treated as functions of  $\xi_{\parallel}$ , with  $\xi_{\perp}(\xi_{\parallel})$  and  $c(\xi_{\parallel})$  set by their relations in pure 8CB. Thus, each fit has only five free parameters,  $q_0$ ,  $A(T)$ ,  $\xi_{\parallel}$ ,  $\sigma_1$ , and  $a_2$ , with two parameters  $\xi_{\parallel}$  and  $a_2/\sigma_1$  controlling the shape of the peaks.

We note that the line shapes of the smectic peaks in Figs. 1–3 are nearly symmetric in  $q$  about the peak position. Such highly symmetric shapes are, in general, not expected from powder averaging Eq. (1), and we interpret this symmetry as a consequence of the relative values of  $\xi_{\perp}$ ,  $\xi_{\parallel}$ , and  $c$ , which conspire to produce such a shape. To illustrate this point, Fig. 4 shows the measured scattering peak from smectic fluctuations in pentylphenylthiol-octyloxybenzoate ( $\bar{8}S5$ ) confined in an aerosil gel with  $\rho_S=0.030$  at 2.56 K above the  $N$ -SmA transition temperature of pure  $\bar{8}S5$ . For a given  $\xi_{\parallel}$ , the quartic coefficient  $c$  is considerably smaller in  $\bar{8}S5$  than in 8CB. This difference leads to a more asymmetric shape of the

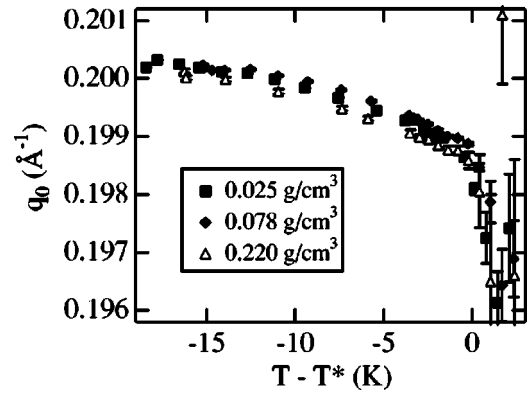


FIG. 5. The ordering wave vector  $q_0$  extracted from the fits with Eqs. (1) and (2) for smectic correlations in 8CB confined in aerosil gels with three  $\rho_S$  values as specified. Temperature is plotted as the difference from  $T^*$ , the onset temperature for static fluctuations. Values for  $T^*$  are given in the inset of Fig. 7.

powder average of the thermal term in Eq. (1). The solid line in Fig. 4 is a fit with Eqs. (1) and (2) with  $a_2=0$  [32], so that only the thermal term is included in describing the smectic fluctuations above  $T_{NA}$ .

While the symmetry in the line shape for 8CB in aerosil highlights the importance of including a quartic term ( $c > 0$ ) in Eq. (1) to account correctly for the measured forms, we stress that the smectic correlations transverse to the nematic director cannot be determined quantitatively with high precision by the measurements. The powdered nature of the liquid crystal in aerosil restricts measurements to effectively longitudinal wave vectors, and the behavior transverse to the director enters only through distortions in the intrinsic form due to the powder averaging. Further, these distortions have their most pronounced effect in the far wings of the line shape, which are obscured by the background scattering from the aerosil. Consequently, the measurements cannot demonstrate with certainty that Eq. (1), with  $\xi_{\perp}(\xi_{\parallel})$  and  $c(\xi_{\parallel})$  identical to pure 8CB, is unique in describing the data. For example, the spatially isotropic disorder of the aerosil could lead to a decrease in the ratio  $\xi_{\parallel}/\xi_{\perp}$ , which ranges approximately from 4 to 15 for pure 8CB, to a value closer to 1, as recent theory indicates [6]. However, as Fig. 3 illustrates, Eqs. (1) and (2) with  $\xi_{\perp}(\xi_{\parallel})$  and  $c(\xi_{\parallel})$  set by pure 8CB values describe the data accurately over the entire investigated range of densities and temperatures. Therefore, this description of the smectic phase with quenched disorder, which in some sense represents a minimal departure from the pure system, is fully consistent with the data.

In measurements on pure 8CB above  $T_{NI}^0$ , we observe a very broad liquid structure peak near  $0.3$  Å<sup>-1</sup>. This feature vanishes in the nematic phase below  $T_{NI}^0$ . Careful measurements also revealed evidence of this peak at high temperatures in 8CB confined in aerosil gels. We note that this feature introduces a small inconsistency in our treatment of the background in Eq. (2). Specifically,  $B(q)$  is obtained from the scattering intensity above  $T_{NI}$ , but any high-temperature liquid-crystal contribution should not be included as part of the background below  $T_{NI}$ . However, we have found that the liquid-crystal contributions to  $B(q)$  are sufficiently small so

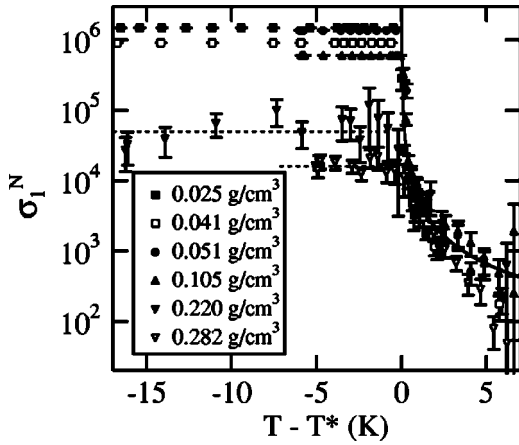


FIG. 6. Amplitude of the thermal fluctuations,  $\sigma_1^N$ , for 8CB confined in aerosil gels of several densities  $\rho_S$  as specified. Temperature is plotted as the difference from  $T^*$ , the onset temperature for static fluctuations. Values for  $T^*$  are given in the inset of Fig. 7. The solid line is the temperature dependence of the susceptibility for pure 8CB, with  $T^*(\text{pure}) = T_{NA}^0$ .

that including or excluding them does not influence the characterization of the smectic peaks at  $q \approx 0.2 \text{ \AA}^{-1}$ . The relative strengths of the aerosil and liquid-crystal scattering can, however, provide a method for normalizing the scattering intensity and thus for comparing the intensities from different samples. In particular, we decompose  $B(q)$  into two separate contributions:

$$I(q, T > T_{NI}^0) = B(q) = v_S B_S(q) + v_{LC} B_{LC}(q), \quad (3)$$

where the shape of the liquid-crystal contribution,  $B_{LC}(q)$ , is obtained from measurements on pure 8CB, and the aerosil gel contribution  $B_S(q)$  is assumed to have a simple power-law form [7]. The ratio of the prefactors  $v_{LC}/v_S$  scales with the aerosil volume fraction as expected [33]. The prefactor to the liquid-crystal contribution,  $v_{LC}$ , which is proportional to the quantity of 8CB in the beam, provides a method for placing the scattering intensities on an absolute scale. We define normalized strengths for the thermal and static fluctuation terms by

$$\sigma_1^N = \sigma_1 / v_{LC}, \quad (4)$$

$$a_2^N = a_2 / v_{LC}, \quad (5)$$

which give the sizes of the two terms for each sample normalized by the scattering volume of 8CB for that sample.

### B. Smectic layer spacing

The wave vector  $q_0$  in Eq. (1) characterizes the spacing of the smectic layers, and Fig. 5 displays the values of  $q_0$  extracted from fits for three aerosil densities. At high temperatures, where the smectic peak has a large width and small amplitude, the scatter in  $q_0$  is too large to determine confidently any systematic dependence on temperature or  $\rho_S$ . At

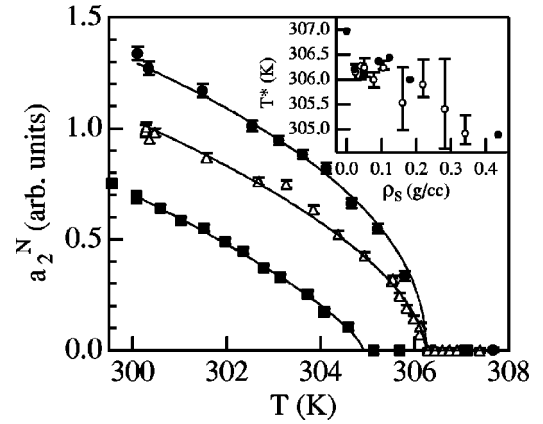


FIG. 7. The integrated area  $a_2^N$  of the static fluctuation term in  $S(q)$  for three values of  $\rho_S$ : 0.051 (solid circles), 0.105 (open triangles), and 0.341 (solid squares). The values for  $\rho_S = 0.051 \text{ g/cm}^3$  and  $\rho_S = 0.105 \text{ g/cm}^3$  have been multiplied by 7 and 5, respectively, for clarity. The solid lines are fits with Eq. (6). The open circles in the inset are the values of  $T^*$ , the onset temperature for static fluctuations extracted from these fits, as a function of  $\rho_S$ . The solid circles in the inset are the peak positions in the specific heat as obtained from calorimetry studies [7].

low temperatures,  $q_0$  appears to be virtually independent of  $\rho_S$  and increases slightly with decreasing temperature. This temperature dependence is shown in Fig. 5 as a function of the difference in temperature from  $T^*$ , the temperature below which the magnitude of static smectic fluctuations becomes nonzero. The procedure for obtaining  $T^*$  and its value as a function of  $\rho_S$  are discussed below in Sec. III D.

The temperature dependence for  $q_0$  was also measured for pure 8CB below  $T_{NA}^0$ . Due to small systematic uncertainties introduced by variations in the x-ray optics, precise comparisons on an absolute scale between the values of  $q_0$  for pure 8CB and those for the aerosil samples could not be made. However,  $q_0$  for the aerosil samples at low temperatures and for pure 8CB in the smectic phase showed very similar temperature dependencies, and we estimate that for a given effective temperature difference,  $T - T^*$ , the fractional difference in  $q_0$  between pure 8CB and any aerosil sample is not more than 0.2%. Thus, the presence of the aerosil has little, if any, effect on the partial bilayer smectic layer spacing in 8CB.

### C. Thermal fluctuations

The amplitude of the thermal fluctuation term,  $\sigma_1^N$ , is displayed in Fig. 6 as a function of temperature for several values of  $\rho_S$ . Consistent with Figs. 2(b) and 2(c), the temperature dependence of  $\sigma_1^N$  at temperatures well above  $T^*$  tracks that of the susceptibility for pure 8CB, which is shown by the solid line in the figure. However, unlike the pure system, where the susceptibility diverges at  $T_{NA}^0$ ,  $\sigma_1^N$  for 8CB confined in aerosil gels remains finite through the “transition” region.

At temperatures below  $T^*$ ,  $\sigma_1^N$  exhibits a roughly temperature-independent value. In Fig. 6,  $\sigma_1^N$  for the  $\rho_S = 0.220$  and  $\rho_S = 0.282$  samples are shown as free parameters

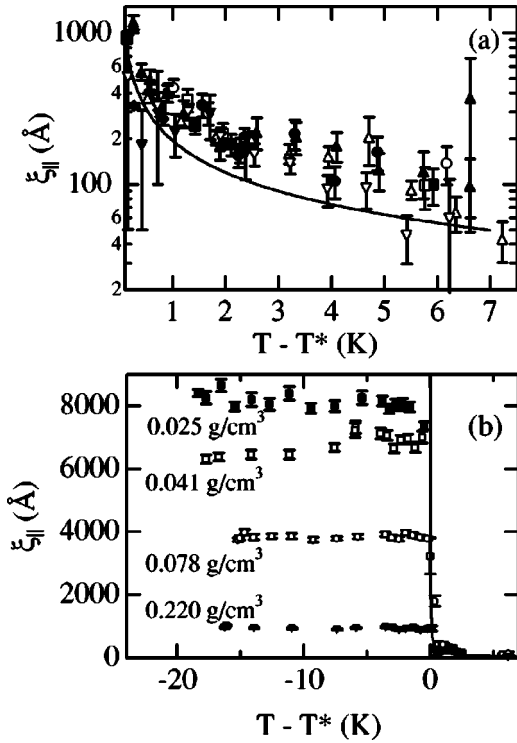


FIG. 8. The smectic correlation length  $\xi_{||}$  for 8CB confined in aerosil gels. (a)  $\xi_{||}$  for  $T > T^*$  compared with that of pure 8CB [solid line with  $T^*(\text{pure}) = T_{NA}^0$ ] for values of  $\rho_S$  as specified in Fig. 9. (b)  $\xi_{||}$  values at low temperatures for four values of  $\rho_S$ .

to low temperatures in order to illustrate the very weak temperature dependence at low  $T$ . Below the pseudotransition region near  $T^*$ , the thermal term should be dominated by long-wavelength excitations, and the scattering intensity from these contributions should be dictated by the Bose occupation factor, which gives  $\sigma_1^N(T) \propto T$ . Over the narrow absolute temperature range ( $\approx 290$  K–307 K) below  $T^*$ , the roughly constant behavior for  $\sigma_1^N$  is consistent with this expectation. On the basis of this observed low-temperature  $\sigma_1^N$  behavior in unconstrained fits, we have repeated the fitting with Eqs. (1) and (2) for each  $\rho_S$  for  $T < T^*$  with  $\sigma_1^N$  fixed at the average low-temperature value for that density. This second iteration of fitting was designed to obtain better stability in the results for the other fit parameters (namely,  $a_2^N$  and  $\xi_{||}$ ) that are coupled to  $\sigma_1^N$  [34]. The results for  $\rho_S = 0.025, 0.041, 0.051,$  and  $0.105$  in Fig. 6 show  $\sigma_1^N$  held constant at low temperature under this procedure. Near and above  $T^*$ , we treat  $\sigma_1^N$  as a free, temperature-dependent parameter, leading to the behavior shown in Fig. 6.

#### D. Static fluctuations

As mentioned above, the scattering intensity from 8CB in aerosil gels above  $T_{NA}^0$  is well described by thermal fluctuations alone, and the static term in Eq. (1) is effectively zero. With decreasing temperature, the contributions from static fluctuations rise sharply from zero. Figure 7 displays the temperature dependence of the static fluctuation term  $a_2^N$  for three values of  $\rho_S$ . The solid lines in the figure are the results of fits with the form

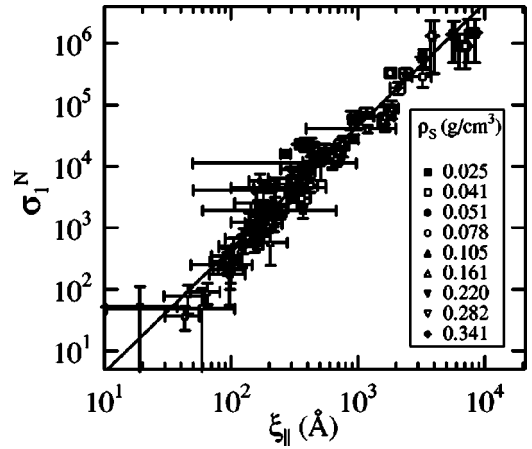


FIG. 9. Amplitude of the thermal fluctuations,  $\sigma_1^N$ , versus correlation length  $\xi_{||}$  for 8CB confined in aerosil gels. The plotted values span the full experimental range of  $\rho_S$  and temperature. The solid line is the relation  $\sigma_1^N \propto \xi_{||}^2$ .

$$a_2^N = B(T^* - T)^x, \quad (6)$$

where  $B$ ,  $x$ , and  $T^*$  depend on  $\rho_S$ . Values for  $B$ ,  $x$ , and  $T^*$  are tabulated in Paper II. As the figure illustrates, this expression describes the temperature dependence of  $a_2^N$  quite well. The significance of this functional form is discussed in Sec. IV.

Fits with Eq. (6) provide unambiguously the onset temperature  $T^*$  of static fluctuations induced by the quenched disorder. The open symbols in the inset of Fig. 7 are the resulting  $T^*$  values as a function of  $\rho_S$ . As the inset illustrates, the onset of static smectic order becomes increasingly suppressed in temperature as  $\rho_S$  increases. This suppression in  $T^*$  quantitatively tracks the decreasing position of the peak in the heat capacity with  $\rho_S$  observed in calorimetry studies [7] and shown in the inset with solid symbols. Due to the considerable uncertainty in the values of  $T^*$  extracted from the fits with Eq. (6), the nonmonotonic variation in “transition” temperature with  $\rho_S$  that was observed calorimetrically for  $\rho_S < 0.1$  [7] cannot be resolved.

#### E. Smectic correlation length

Consistent with Figs. 2(b) and 2(c), the values of the smectic correlation lengths  $\xi_{||}$ , extracted from the fits with Eqs. (1) and (2) for  $T > T^*$ , are like those of pure 8CB and track its temperature dependence. Figure 8(a) displays  $\xi_{||}$  at temperatures above  $T^*$ . Any possible systematic variation in  $\xi_{||}$  with  $\rho_S$  is overwhelmed by the scatter in the data. The solid line in the figure is  $\xi_{||}$  for pure 8CB [26], where we use  $T_{NA}^0$  for  $T^*$ . A detailed scaling analysis of the temperature dependence expected for  $\xi_{||}$  of 8CB+aerosils above  $T^*$  is provided in Paper II.

As with  $\sigma_1^N$ ,  $\xi_{||}$  for aerosil samples fails to track the diverging behavior of the pure system through  $T_{NA}$  and remains finite to low temperature. At temperatures below  $T^*$ ,  $\xi_{||}$  approaches an essentially temperature-independent value. Figure 8(b) shows the correlation lengths at low temperature for four densities of aerosil. The variation of the low-

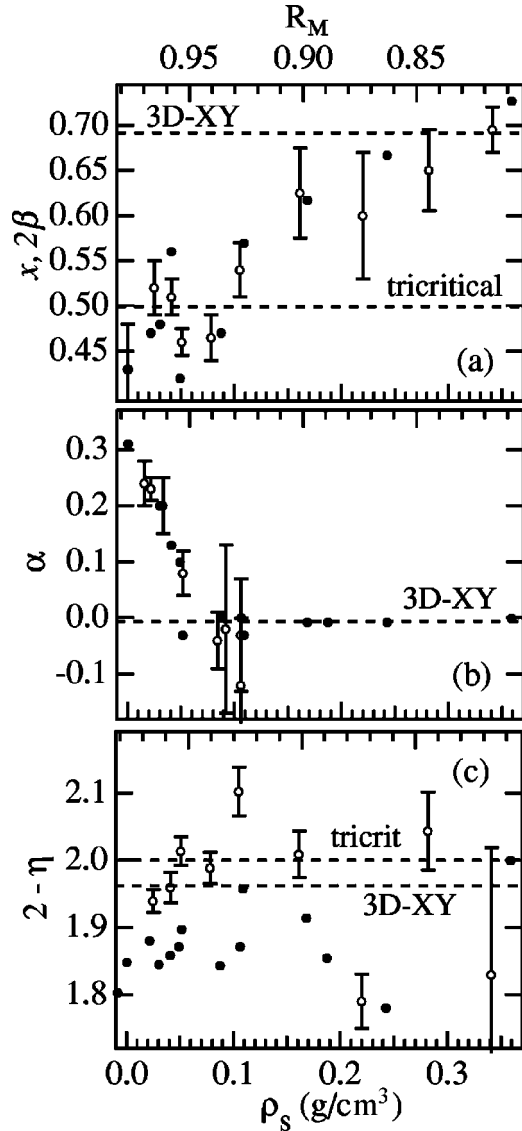


FIG. 10. (a) The effective exponent  $x$  from fits to  $a_2(T)$  with Eq. (6) for 8CB+aerosil samples (open circles) versus  $\rho_S$ . Also given are values of the squared order parameter exponent  $2\beta$  (filled circles) for a series of pure liquid crystals with varying MacMillan ratios  $R_M \equiv T_{NA}/T_{NI}$ , as determined from data given in Ref. [35]. The effective exponent  $x$  spans the range from near a tricritical value,  $2\beta=0.5$ , at small  $\rho_S$  to a 3D XY-like value,  $2\beta=0.691$ , at large  $\rho_S$ . (b) The effective exponent  $\alpha$  from calorimetric studies on 8CB confined in aerosil gels [7] (open circles) along with values of  $\alpha$  (filled circles) for a series of pure liquid crystals with varying  $R_M$ , as given in Ref. [35]. (c) The effective exponent  $2-\eta$  obtained from fits with the form  $\sigma_1^N = A\xi_{\parallel}^{2-\eta}$  versus  $\rho_S$  (open circles) and the critical exponent  $\gamma/\nu_{\parallel} (=2-\eta_{\parallel})$  for a series of pure liquid crystals as a function of  $R_M$ . Note that the linear scaling between  $\rho_S$  and  $R_M$ , given by Eq. (8), is the same for all three plots.

temperature correlation length  $\xi_{\parallel}^{LT} \equiv \xi_{\parallel}(T \ll T^*)$  with  $\rho_S$  is described in Sec. IV.

#### IV. DISCUSSION

As the results outlined in Sec. III demonstrate, confinement by aerosil gels strongly affects the smectic transition in

8CB. The success of Eq. (1) indicates that these effects can be modeled as random fields. Consistent with theoretical predictions, the random fields destroy the transition to a quasi-long-range-ordered smectic phase and replace it with the formation of short-ranged correlations. In this section, we investigate the relationship between the strength of this disorder and the corresponding short-ranged smectic order, including possible connections with theoretical predictions, as well as aspects of the pseudocritical behavior exhibited by 8CB confined in aerosil gels.

#### A. Pseudocritical behavior

As Figs. 6 and 8(a) illustrate, the smectic scattering in 8CB confined in aerosil gels above  $T^*$  resembles, to a first approximation, thermal critical fluctuations unaffected by quenched disorder. This close connection between the thermal term in Eq. (1) for 8CB+aerosils and the corresponding term for pure liquid crystals in the nematic phase is strengthened by considering the scaling relation between  $\sigma_1^N$  and  $\xi_{\parallel}$ . In a pure isotropic critical system for  $T > T_c$ , one has  $\sigma_1 \propto t^{-\gamma}$  and  $\xi \propto t^{-\nu}$ , which leads to  $\sigma_1 \propto \xi^{\gamma/\nu} = \xi^{2-\eta}$ . For liquid crystals, which exhibit critical anisotropy in the behavior of the correlation lengths, one obtains  $\sigma_1 \propto \xi_{\parallel}^{\gamma/\nu_{\parallel}}$ , where  $\gamma/\nu_{\parallel} = 2 - \eta_{\parallel}$ . This scaling relation between the thermal susceptibility and the parallel correlation length for 8CB+aerosils can be written as

$$\sigma_1^N = A \xi_{\parallel}^{2-\eta}, \quad (7)$$

where the subscript on  $\eta$  has been dropped for convenience. Figure 9 displays a log-log plot of  $\sigma_1^N$  versus  $\xi_{\parallel}$  for a series of samples of varying  $\rho_S$  and a line representing  $\sigma_1 \propto \xi_{\parallel}^2$ . As the figure demonstrates, the scaling relation holds for 8CB confined in aerosil gels over the entire experimental temperature range, both in the pseudocritical regime above  $T^*$  and at low temperature, where both  $\sigma_1^N$  and  $\xi_{\parallel}$  have only weak temperature dependence. Further, the scaling amplitude  $A$  shows no systematic variation with  $\rho_S$ . Indeed, the successful collapse of data from different samples in Fig. 9 suggests the validity of the normalization procedure for  $\sigma_1^N$  using  $\nu_{LC}$ . Also clear from the figure is the fact that  $2-\eta$  is close to 2 for 8CB+aerosils. The mean field and the Gaussian tricritical value of  $2-\eta$  is 2.00, and the 3D XY value is 1.962. Furthermore, the value of  $\gamma/\nu_{\parallel}$  is 1.88 for pure 8CB [26]. The correspondence between the scaling given in Eq. (7) applied to 8CB+aerosil gels of varying  $\rho_S$  and that for pure liquid crystals is discussed below.

This pseudocritical behavior of 8CB confined in aerosil gels also extends below  $T^*$ , where  $c$  in Eq. (1) approaches a small constant value, and  $a_2$  becomes proportional to the integrated intensity of the static fluctuation term in  $I(q)$ . The growth of this intensity, shown in Fig. 7, strongly resembles that of an order parameter squared, as the success of the fits of  $a_2$  with Eq. (6) illustrates. Figure 10(a) shows the values of the effective exponent  $x$  extracted from these fits as a function of  $\rho_S$ . For pure liquid crystals, the critical behavior observed at the  $N$ -SmA transition is affected by the proxim-

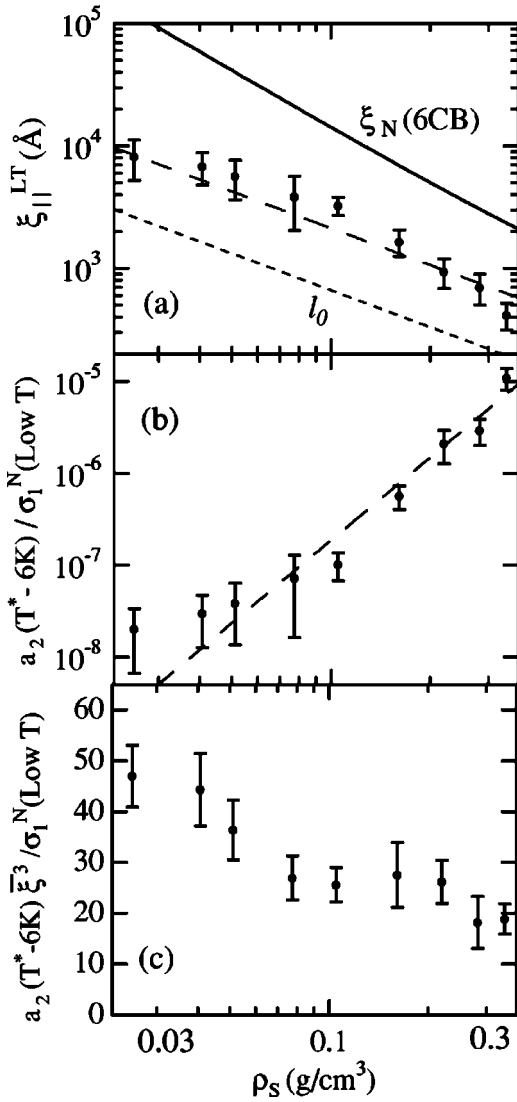


FIG. 11. (a) Low-temperature correlation length  $\xi_{||}^{LT}$  as a function of  $\rho_S$ . The solid line is the nematic correlation length (for 6CB) measured by static light scattering [10], and the dashed line is the mean aerosil void size  $l_0$ . The long-dashed line represents the form  $\xi_{||}^{LT} \propto \rho_S^{-1}$ . (b) The ratio  $a_2^N / \sigma_1^N(\text{low } T)$  at the fixed temperature difference  $T^* - T = 6$  K as a function of  $\rho_S$ . The long-dashed line is the relation  $a_2^N / \sigma_1^N(\text{low } T) \propto \rho_S^3$ . (c) The ratio  $a_2^N \bar{\xi}^3 / \sigma_1^N(\text{low } T)$  at the fixed temperature difference  $T^* - T = 6$  K as a function of  $\rho_S$ .

ity of the higher-temperature nematic to isotropic transition through a coupling between the nematic and smectic order parameters (e.g., de Gennes coupling; see Paper II) [35]. The strength of this coupling depends on the magnitude of the nematic susceptibility at  $T_{NA}$ , which for pure liquid crystals depends on the width of the nematic range and can be roughly parametrized by the MacMillan ratio,  $R_M \equiv T_{NA} / T_{NI}$ . When  $R_M$  becomes small ( $R_M \approx 0.7$ ), the  $N$ -SmA transition is observed to approach 3D  $XY$  behavior but still exhibits a small anisotropy in the critical correlations [36], while it approaches tricritical behavior and then becomes first order as  $R_M \rightarrow 1$  [35]. Values of  $2\beta$ , determined

through the Rushbrooke scaling equality  $2\beta = 2 - \alpha - \gamma$  [37], for a series of pure liquid crystals [35] with varying  $R_M$ , are included in Fig. 10(a). The effective 8CB+aerosil exponents  $x$  span the range from near the tricritical value  $2\beta = 0.5$  (like pure 8CB) at small  $\rho_S$  to 3D  $XY$ -like,  $2\beta = 0.691$ , at large  $\rho_S$ . With increasing  $\rho_S$ , the quenched disorder has the apparent effect of suppressing the nematic susceptibility and thus the coupling that drives the critical behavior of the  $N$ -SmA transition in pure liquid crystals away from 3D  $XY$  universality.

This trend agrees very closely with the corresponding behavior observed in specific heat studies of 8CB with dispersed aerosils [7]. Figure 10(b) shows the values of the effective heat capacity exponent  $\alpha$  from the calorimetric study versus  $\rho_S$ . As the figure illustrates,  $\alpha$  decreases toward the 3D  $XY$  value with increasing  $\rho_S$ . The solid circles in Fig. 10(b) are the critical exponents measured for pure liquid crystals as a function of  $R_M$ . The same linear scaling between  $\rho_S$  and  $R_M$  successfully collapses the aerosil data onto the pure liquid crystals in Figs. 10(a) and 10(b) and suggests the notion of an effective MacMillan ratio for 8CB in aerosil gels,

$$R_M^{eff}(\text{sil}) = 0.977 - 0.47\rho_S. \quad (8)$$

This general relationship between  $R_M^{eff}(\text{sil})$  and  $\rho_S$  for two distinct pseudocritical behaviors strengthens the idea that the presence of quenched disorder suppresses the nematic susceptibility in 8CB near  $T^*$ . This suppression likely results from the role of surface anchoring on the gel strands in changing the properties of the nematic phase, since the observed ratio  $T_{NA} / T_{NI}$  for 8CB+aerosils varies little with  $\rho_S$  [7]. Figure 10(c) displays values of  $2 - \eta_{||}$  extracted from fits with Eq. (7) to  $\sigma_1^N$  and  $\xi_{||}$  values obtained for different  $\rho_S$  samples. Also shown in Fig. 10(c) are values of  $\gamma / \nu_{||}$  ( $= 2 - \eta_{||}$ ) for pure liquid crystals as a function of  $R_M$ . Due to the small difference in  $2 - \eta_{||}$  between the tricritical and 3D  $XY$  values and the large scatter in the results both for pure liquid crystals and for 8CB+aerosil samples, systematic trends like those seen in Figs. 10(a) and 10(b) are less clear for  $2 - \eta_{||}$ . Tabulated values for  $2 - \eta_{||}$  are given in Paper II.

## B. Low-temperature correlations

As Fig. 8(b) demonstrates, the correlation length for smectic order in 8CB confined in aerosil gels saturates at low temperature. Figure 11(a) shows these low-temperature parallel correlation lengths  $\xi_{||}^{LT}$  as a function of  $\rho_S$ . The solid line in Fig. 11(a) shows the trend in the nematic correlation lengths of the homolog 6CB with dispersed aerosils, as measured by Bellini *et al.* [10] with static light scattering. These light scattering studies demonstrate that the nematic order in a liquid crystal with dispersed aerosil breaks up into very large, but finite, domains. Since smectic layering forms within regions with nematic order, the nematic domain sizes set upper limits for the range of the smectic correlations. However,  $\xi_{||}^{LT}$  remains well below these limits for all  $\rho_S$ , demonstrating the sensitivity of the smectic phase to quenched disorder. The dashed line in Fig. 11(a) is the mean

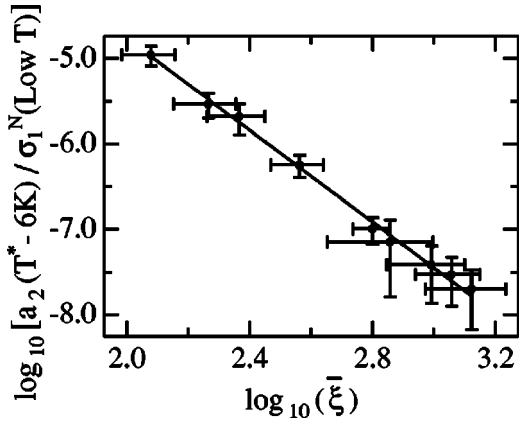


FIG. 12. The ratio  $a_2^N/\sigma_1^N(\text{low}T)$  at the fixed temperature difference  $T^* - T = 6$  K as a function of  $\bar{\xi}$ . The solid line is a power-law fit giving an exponent value of  $-2.68$ .

aerosil void size  $l_0$  as a function of  $\rho_S$  [7,21]. Over the range of densities studied,  $\xi_{\parallel}^{LT}$  exceeds  $l_0$  by a factor of 3 or more, consistent with an intermediate strength disordering field. Paper II provides a detailed discussion of the role of  $l_0$  in setting the range of the smectic correlations.

Figure 11(b) displays  $a_2^N/\sigma_1^N$  as a function of  $\rho_S$  for  $T = T^* - 6$  K. We plot this ratio rather than  $\sigma_1^N$  or  $a_2^N$  alone to characterize the magnitude of the fluctuations, in order to remove any errors that the uncertainties in  $v_{LC}$  might introduce through the normalization. Because the exponent  $x$  characterizing the growth of  $a_2^N$  below  $T^*$  is only weakly dependent on  $\rho_S$ , the trends observed for this ratio are insensitive (on a logarithmic scale) to the temperature difference  $T^* - T$  used to evaluate  $a_2^N$ . Figure 11(c) shows the quantity  $a_2^N \bar{\xi}^3 / \sigma_1^N$ , where  $\bar{\xi} \equiv (\xi_{\parallel} \xi_{\perp}^2)^{1/3}$  is the mean correlation length at low temperature. This quantity, which is approximately the ratio of the integrated intensities of the thermal and disorder terms at low temperature, shows little variation with  $\rho_S$ .

### C. Comparisons with theory

As mentioned in the Introduction, random-field models have served as important examples for understanding possible consequences of quenched disorder, and extensive theoretical work has been devoted to random-field systems. For the case of transitions that break a continuous symmetry in three dimensions, such as the nematic to smectic-A transition, the domain wall energy arguments of Imry and Ma conclude that the transition is unstable to arbitrarily weak random fields [13]. Subsequent theoretical work has rigorously established this conclusion [15], consistent with the short-ranged smectic order measured for all 8CB+aerosil samples well below  $T_{NA}^0$ . For quantitative comparisons with these short-range smectic correlations, two theoretical efforts provide guidance. In the first, Aharony and Pytte [14] apply scaling arguments to predict the low-temperature form of the structure factor for systems with transitions breaking continuous symmetries in the presence of random fields. In the

second, Radzihovsky and Toner [17] develop a detailed theory for smectics with random quenched disorder.

The strength of the disorder imposed on smectic 8CB by confinement in aerosil gels clearly correlates with the density of the aerosil; however, the precise relation between density and disorder is unknown. Within the simplest assumption, confinement in the gels induces random fields whose disorder strength is proportional to the gel density. With this assumption, the scaling arguments of Aharony and Pytte predict  $\xi \propto \Delta^{-1} \propto \rho_S^{-1}$ , where  $\Delta$  is the strength of the random-field disorder. The exponent  $-1$  is obtained from  $-1/(d_c - d)$  where  $d=3$  is the spatial dimension and  $d_c=4$  is the lower critical dimension for the random field XY model [38]. The long-dashed line in Fig. 11(a) is the power-law form  $\xi_{\parallel}^{LT} \propto \rho_S^{-1}$ . Over the range of  $\rho_S$  covered experimentally, measured values of  $\xi_{\parallel}^{LT}$  appear roughly to follow this behavior. A best fit to a power-law form over the full range of  $\rho_S$  gives  $\xi_{\parallel}^{LT} \propto \rho_S^{-1.1 \pm 0.2}$ . The scaling arguments of Aharony and Pytte further lead to  $a_2^N/\sigma_1^N \propto \Delta^3$ . The long-dashed line in Fig. 11(b) is this relation, again assuming  $\Delta \propto \rho_S$ . As with  $\xi_{\parallel}$ ,  $a_2^N/\sigma_1^N$  follows a trend crudely consistent with the predicted power-law behavior, but clear deviations from the predicted form are also apparent. One possible source for these discrepancies could be a more subtle relation between  $\rho_S$  and the disorder strength. Paper II elaborates on this issue.

In order to make comparisons that are free of the dependence of disorder on  $\rho_S$ , we plot in Fig. 12  $a_2^N/\sigma_1^N$  against  $\bar{\xi}$ . In this plot we use  $\bar{\xi}$  rather than  $\xi_{\parallel}$  since the scaling theory is for an isotropic system, and  $\bar{\xi}^3$  represents the correlation volume. According to the scaling theory,  $a_2^N/\sigma_1^N$  should vary with correlation length like  $\bar{\xi}^{-3}$ , while a best fit shown by the solid line gives  $\bar{\xi}^{-2.68 \pm 0.26}$ . This relatively good agreement with the theory is also reflected in the weak variation with the disorder strength of  $a_2^N \bar{\xi}^3 / \sigma_1^N$  shown in Fig. 11(c).

A second possible source of discrepancy between the smectic correlations in 8CB+aerosil and the scaling arguments of Aharony and Pytte is that additional disordering effects enter the confined smectic beyond those of the random-field 3D XY system. In their discussion of smectic liquid crystals with quenched disorder, Radzihovsky and Toner identify two sources of disorder: tilt disorder, which couples to orientation (i.e., the nematic director), and a layer displacement disorder, which couples directly to the smectic order parameter. While the latter corresponds to the disorder of the XY model, the former is predicted to be the dominant disorder for the smectic. An important prediction of the work of Radzihovsky and Toner is that the disordered smectic should possess anomalous elasticity, and one consequence of this prediction is that the correlation length ratio  $\xi_{\parallel}/\xi_{\perp}$  is reduced from that of the pure system. In our modeling of the smectic correlations with Eq. (1), we find that maintaining  $\xi_{\parallel}/\xi_{\perp}$  equal to its values in pure 8CB produces good fits to the data. However, the powder nature of the measured line-shapes creates considerable uncertainties in  $\xi_{\perp}$ , so that we can not exclude some reduction in the correlation length ratio. Despite this inconsistency, the prediction from Radzihovsky and Toner that  $\xi_{\parallel}^{LT} \propto \Delta^{-1}$  is roughly consistent with

our results in Fig. 11(a), assuming again  $\Delta \propto \rho_S$  holds approximately.

Radzihovsky and Toner further predict that  $\xi(T) \propto B(T)^{1/\Gamma}$  at low temperature, where  $B(T)$  is the layer compression modulus of the pure liquid crystal. Within this theory,  $1/\Gamma > 1/2$  is required for a smectic Bragg glass phase to be stable. Published data for  $B(T)$  of 8CB extend only 3 K below  $T_{NA}^0$  [39], so a direct test of this scaling prediction is difficult. However, the essentially temperature-independent behavior of  $\xi_{\parallel}$  at low temperature shown in Fig. 8(b) indicates that such scaling does not hold for 8CB in aerosils. We note that this conclusion differs from that reported for 8CB confined in aerogels, in which the analysis of those x-ray scattering results yielded  $\xi(T)$  consistent with  $\xi(T) \propto B(T)^{1/\Gamma}$  and with marginal Bragg glass stability [6]. This contrast between the aerosil and aerogel results is somewhat surprising since the validity of the prediction of a Bragg glass is within a regime of weak disorder, and the aerosil gels impose a more gentle perturbation on the smectic than aerogels. One source for the different  $\xi_{\parallel}(T)$  behaviors could be the partial compliance of the aerosil gel with the elasticity of the liquid crystal, a feature that is not incorporated into the theory and may complicate comparisons with it. However, a number of differences also exist between the approach used for analyzing the smectic line shapes in the aerogel study [3,6] and the analysis presented here for aerosil samples. For 8CB+aerosil data, analysis such as that used in the aerogel study has strong consequences for  $\xi(T)$ . Further study of other liquid crystals would clearly help in determining whether the contrast between the aerogel and aerosil systems in their agreement with Bragg glass stability is a consequence of elastic coupling that is not considered in the theory or, perhaps, an artifact of the differing approaches to the line-shape analysis. Such studies would also be invaluable in testing the generality of trends observed for 8CB, such as the crossover to 3D XY behavior shown in Fig. 10, with the

introduction of quenched disorder through confinement in aerosil.

## ACKNOWLEDGMENTS

We thank S. Lamarra for technical support and P. Clegg and L. Radzihovsky for helpful discussions. This work was supported by the Natural Science and Engineering Research Council of Canada (Toronto) and by the NSF under CAREER Grant No. DMR-0134377 (JHU), CAREER Grant No. DMR-0092786 (WPI), and Contract No. DMR-0071256 (MIT).

## APPENDIX: ANALYTIC POWDER AVERAGING OF THE SMECTIC STRUCTURE FACTOR

The x-ray structure factor for the smectic fluctuations in 8CB confined by aerosil gels, given in Eq. (1), includes two terms. The first term (LFC) is an anisotropic Lorentzian with a fourth-order correction in the transverse direction that accounts for critical thermal fluctuations. The second term (LFC2) is proportional to the thermal term squared and accounts for random-field induced static fluctuations. Although an anisotropic Lorentzian raised to a power along the transverse direction,  $S(\mathbf{q}) = \sigma / [\xi_{\parallel}^2 (q_{\parallel} - q_0)^2 + (1 + \xi_{\perp}^2 q_{\perp}^2)^{1 - \eta_{\perp}/2}]$ , is equally successful in describing the thermal fluctuations [40], we use the LFC because its powder average can be calculated analytically. The structure factor for a powdered sample is equivalent to that for a single-domain sample averaged with equal weight over all orientations of the smectic wave vector  $\mathbf{q}_0$ , relative to the scattering wave vector  $\mathbf{q}$ ,

$$S^{powder}(q) = \frac{1}{4\pi} \int d\Omega_{\mathbf{q}_0} S(\mathbf{q}). \quad (\text{A1})$$

For the LFC term, the integral has the form

$$\begin{aligned} S_{LFC}^{powder}(q) &= \frac{1}{4\pi} \int d\Omega_{\mathbf{q}_0} \frac{\sigma}{\{1 + \xi_{\parallel}^2 (q_{\parallel} - q_0)^2 + \xi_{\perp}^2 q_{\perp}^2 + c \xi_{\perp}^4 q_{\perp}^4\}} \\ &= \frac{1}{2} \int_{-1}^1 d \cos \theta \frac{\sigma}{\{1 + \xi_{\parallel}^2 (q \cos \theta - q_0)^2 + \xi_{\perp}^2 q^2 \sin^2 \theta + c \xi_{\perp}^4 q^4 \sin^4 \theta\}} \\ &= \frac{\sigma}{2} \int_{-1}^1 d\mu \frac{1}{(A + 2B\mu + C\mu^2 + D\mu^4)}, \end{aligned} \quad (\text{A2})$$

where

$$A = 1 + \xi_{\parallel}^2 q_0^2 + \xi_{\perp}^2 q^2 + c \xi_{\perp}^4 q^4,$$

$$B = -\xi_{\parallel}^2 q_0 q,$$

$$C = (\xi_{\parallel}^2 - \xi_{\perp}^2) q^2 - 2c \xi_{\perp}^4 q^4,$$

$$D = c \xi_{\perp}^4 q^4. \quad (\text{A3})$$

This integral in turn can be written as

$$S_{LFC}^{powder}(q) = \frac{1}{D} \int_{-1}^1 d\mu \prod_i \frac{1}{(\mu - \alpha_i)_i^m}, \quad (\text{A4})$$

where  $\alpha_i$  are the roots with multiplicity  $m$  of the quartic equation

$$A + 2B\mu + C\mu^2 + D\mu^4 = 0. \quad (\text{A5})$$

With the integrand in this form, it can be expanded into a sum of terms,

$$\prod_i \frac{1}{(\mu - \alpha_i)^m} = \sum_{i, 1 \leq j \leq m} \frac{C_{ij}}{(\mu - \alpha_i)^j}, \quad (\text{A6})$$

where the coefficients  $C_{ij}$  are obtained through the expansion process. At this stage, each term can be evaluated analytically using elementary definite integrals, such as

$$\int_{-1}^1 d\mu \frac{1}{\mu - \alpha} = \frac{1}{2} \ln \left| \frac{(1 - \alpha_R)^2 + \alpha_I^2}{(1 + \alpha_R)^2 + \alpha_I^2} \right| + i \left[ \tan^{-1} \left( \frac{1 - \alpha_R}{\alpha_I} \right) + \tan^{-1} \left( \frac{1 + \alpha_R}{\alpha_I} \right) \right], \quad (\text{A7})$$

where  $\alpha = \alpha_R + i\alpha_I$ .

The analytic powder averaging of the LFC2 term follows the same approach:

$$\begin{aligned} S_{LFC2}^{powder}(q) &= \frac{1}{4\pi} \int d\Omega_{q_0} \frac{\sigma}{\{1 + \xi_{\parallel}^2 (q_{\parallel} - q_0)^2 + \xi_{\perp}^2 q_{\perp}^2 + c \xi_{\perp}^4 q_{\perp}^4\}^2} \\ &= \frac{\sigma}{2} \int_{-1}^1 d\mu \frac{1}{(A + 2B\mu + C\mu^2 + D\mu^4)^2} \\ &= \frac{\sigma}{2D^2} \int_{-1}^1 d\mu \prod_i \frac{1}{(\mu - \alpha_i)^{2m_i}}. \end{aligned} \quad (\text{A8})$$

As with the LFC term, this integral can be expanded into a series of elementary definite integrals.

- 
- [1] L. Wu, B. Zhou, C.W. Garland, T. Bellini, and D.W. Schaefer, *Phys. Rev. E* **51**, 2157 (1995).
- [2] N.A. Clark, T. Bellini, R.M. Malzbender, B.N. Thomas, A.G. Rappaport, C.D. Muzny, D.W. Schaefer, and L. Hrubesh, *Phys. Rev. Lett.* **71**, 3505 (1993).
- [3] A.G. Rappaport, N.A. Clark, B.N. Thomas, and T. Bellini, in *Liquid Crystals in Complex Geometries Formed by Polymer and Porous Networks*, edited by G.P. Crawford and S. Zumer (Taylor & Francis, London, 1996), Chap. 20.
- [4] H. Zeng, B. Zalar, G.S. Iannacchione, and D. Finotello, *Phys. Rev. E* **60**, 5607 (1999).
- [5] T. Bellini, N.A. Clark, and D.W. Schaefer, *Phys. Rev. Lett.* **74**, 2740 (1995).
- [6] T. Bellini, L. Radzihovsky, J. Toner, and N.A. Clark, *Science* **294**, 1074 (2001).
- [7] G.S. Iannacchione, C.W. Garland, J.T. Mang, and T.P. Rieker, *Phys. Rev. E* **58**, 5966 (1998).
- [8] T. Jin and D. Finotello, *Phys. Rev. Lett.* **86**, 818 (2001).
- [9] A. Hourri, T.K. Bose, and J. Thoen, *Phys. Rev. E* **63**, 051702 (2001).
- [10] T. Bellini, N.A. Clark, V. Degiorgio, F. Mantegazza, and G. Natale, *Phys. Rev. E* **57**, 2996 (1998).
- [11] S. Park, R.L. Leheny, R.J. Birgeneau, J.-L. Gallani, C.W. Garland, and G.S. Iannacchione, *Phys. Rev. E* **65**, 050703 (2002).
- [12] R.J. Birgeneau, *J. Magn. Magn. Mater.* **177-181**, 1 (1998).
- [13] Y. Imry and S.-K. Ma, *Phys. Rev. Lett.* **35**, 1399 (1975).
- [14] A. Aharony and E. Pytte, *Phys. Rev. B* **27**, 5872 (1983).
- [15] M. Aizenman and J. Wehr, *Phys. Rev. Lett.* **62**, 2503 (1989).
- [16] D.S. Fisher, *Phys. Rev. Lett.* **78**, 1964 (1997).
- [17] L. Radzihovsky and J. Toner, *Phys. Rev. B* **60**, 206 (1999).
- [18] B. Ward, Ph.D. thesis, University of Colorado, 1999 (unpublished).
- [19] D.S. Fisher, *Phys. Rev. Lett.* **56**, 416 (1986).
- [20] Q. Feng, R.J. Birgeneau, and J.P. Hill, *Phys. Rev. B* **51**, 15 188 (1995).
- [21] G.S. Iannacchione *et al.*, following paper, *Phys. Rev. E*, **67**, 011709 (2003).
- [22] D.E. Feldman, *Phys. Rev. Lett.* **84**, 4886 (2001).
- [23] W. E and P. Palfy-Muhoray, *Phys. Rev. E* **57**, 135 (1998).
- [24] A. Maritan, M. Cieplak, T. Bellini, and J.R. Banavar, *Phys. Rev. Lett.* **72**, 4113 (1994).
- [25] With such a fixed horizontal aperture, the azimuthal acceptance angle decreases as  $1/q$ , in principle distorting the line shape for even an extremely narrow aperture. However, efforts to account for this distortion in the analysis of the smectic line shapes showed that it had negligible effect.
- [26] B.M. Ocko, R.J. Birgeneau, and J.D. Litster, *Z. Phys. B: Condens. Matter* **62**, 487 (1986).
- [27] R.J. Birgeneau, R.A. Cowley, G. Shirane, and H. Yoshizawa, *J. Stat. Phys.* **34**, 817 (1984).
- [28] G. Grinstein, S.-k. Ma, and G.F. Mazenko, *Phys. Rev. B* **15**, 258 (1977).
- [29] D. Andelman and J.-F. Joanny, in *Scaling Phenomena in Disordered Systems*, edited by R. Pynn and A. Skjeltorp (Plenum Press, New York, 1985).
- [30] R.A. Pelcovits and A. Aharony, *Phys. Rev. B* **31**, 350 (1985).
- [31] In the smectic phase, the correlations do not have true long-range order but exhibit algebraic decay due to the Landau-Peierls instability. We do not think this distinction should influence the form of the correlations in the presence of quenched disorder.
- [32] As for the fits made to 8CB+aerosil data,  $\xi_{\perp}$  and  $c$  were taken to have the same functional dependence on  $\xi_{\parallel}$ ,  $\xi_{\perp}(\xi_{\parallel})$ , and  $c(\xi_{\parallel})$ , as in pure 8S5.
- [33] S. Park, Ph.D. dissertation, Massachusetts Institute of Technology, 2001 (unpublished).
- [34] For some of the samples the  $\chi^2_{\nu}$  minimum associated with fitting  $I(q)$  was quite broad. Thus, if  $\sigma_1$ ,  $a_2$ , and  $\xi_{\parallel}$  are all allowed to be free parameters for  $T < T^*$ , there is an artificial and *correlated* "fit noise" in all three parameters that does not

reflect experimental scatter in the  $I(q)$  data.

- [35] C.W. Garland and G. Nounesis, Phys. Rev. E **49**, 2964 (1994), and references therein.
- [36] C.W. Garland, G. Nounesis, M.J. Young, and R.J. Birgeneau, Phys. Rev. E **47**, 1918 (1993).
- [37] The quasi-long-range (algebraic) order of the smectic phase prevents a direct measurement of the order parameter amplitude.
- [38] Following arguments of dimensional reduction [A. Aharony, Y. Imry, and S.K. Ma, Phys. Rev. Lett. **37**, 1364 (1976); A.P. Young, J. Phys. C **10**, L257 (1977)],  $d_c=2$  for the pure  $XY$  model is raised to  $d_c=4$  by the presence of random fields. A 3D  $XY$  scaling analysis of the precritical regime of pure liquid crystals (see Ref. [36]) is quite successful over a range of correlation lengths similar to that probed here. Accordingly, we assume  $XY$  scaling in our liquid-crystal-silica system, which then implies that we should use  $d_c=4$ . Arguments based on the smectic elasticity that predict  $d_c>4$  (see Ref. [17]) may become relevant at asymptotically larger scales.
- [39] M. Benzekri, T. Claverie, J.P. Marcerou, and J.C. Rouillon, Phys. Rev. Lett. **68**, 2480 (1992).
- [40] B.M. Ocko, Ph.D. dissertation, Massachusetts Institute of Technology, 1984 (unpublished).